Chapter 1
Introduction

1.1 Transparency

Transparent materials form a special group of materials that have a wide range of applications in various aspects of our daily life. Transparency, also known as pellucidity or diaphaneity, is a unique physical property of materials, which measures their ability to allow light to pass through them without the presence of scattering. At macroscopic scale, the behavior of the photons follows Snell's law, because this dimension is much larger than the wavelength of photons. Translucency is another property closely related to transparency, which is also known as translucence or translucidity. In this case, the materials allow light to pass through, but Snell's law may not be followed at macroscopic scale. In other words, the photons could be scattered either internally or at the interfaces where the index of refraction is varied. The opposite property of translucency and transparency is opacity. Transparent materials usually have a clear appearance, either in one color or any combination leading to a spectrum of multiple colors. When light shines on a material, they could have several interactions, which are dependent on both the wavelength of the light and the nature of the material. Photons interact with an object in the forms of reflection, absorption, and transmission [1].

1.2 Transparent Materials

Conventional materials that are optically transparent mainly include glasses, polymers, and alkali hydrides, which have various applications in industries and daily life. However, these materials have relatively poor mechanical strength and sometimes insufficient chemical and physical stabilities. More importantly, conventional transparent materials have strong absorption in the IR range, making them not suitable for applications in this spectral range. Also, they usually possess

L.B. Kong et al., *Transparent Ceramics*, Topics in Mining,
Metallurgy and Materials Engineering, DOI 10.1007/978-3-319-18956-7_1

relatively low melting temperatures (<600 °C), so that they cannot be used for applications at high temperatures. As a result, it is desirable to develop new transparent materials that can be used for applications operating in harsh and extreme environments.

With the advancement in technologies in material growth, single crystals of some compounds appeared as new transparent materials. Compared with conventional transparent materials, single crystals, such as sapphire (Al_2O_3) for IR windows, YAG (yttrium garnet, $Y_3Al_5O_{12}$) for lasers, and PZN-PT (lead zinc niobate-lead titanate, $PbZn_{1/3}Nb_{2/3}O_3$-$PbTiO_3$) for electro-optics, addressed most of the problems encountered by conventional transparent materials. However, growth of single crystals requires sophisticated facilities and is time-consuming, thus leading to expensive products that are only used in the case cost is not necessarily considered. Furthermore, as-grown single crystals have shapes determined more by their lattice structures and less by processing conditions. Therefore, machining of single crystals to meet the requirement of specific applications is a difficult task. Other problems of single crystals include difficulty of large-scale production and mechanical brittleness of some materials. In this respect, transparent ceramics become more and more important. Transparent ceramics have various advantages over single crystals, such as cost-effectiveness, large-scale production, feasibility of shape controlling, and better mechanical properties.

Different from single crystals, ceramics have various sites to scatter light, including residual pores within grains and at grain boundaries, grain boundaries, second phases (impurities) at the grain boundaries, and double refraction from birefringent materials, as shown schematically in Fig. 1.1 [2].

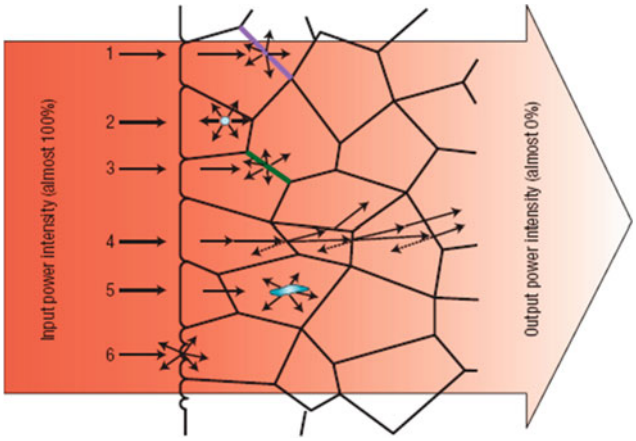

Fig. 1.1 Schematic microstructure of a ceramic with various light-scattering sources: (*1*) a grain boundary, (*2*) residual pores, (*3*) secondary phase, (*4*) double refraction, (*5*) inclusions and (*6*) surface roughness in ceramics prohibits applications in optics. Reproduced with permission from [3]. Copyright © 2008, Nature Publishing Group

The most significant factor for transparency of ceramics is porosity. The surface of a pore is a boundary between phases with sharply different optical characteristics, which therefore intensely reflects and refracts light. The presence of a large number of pores makes ceramics opaque. Pores could be interbrain or intragrain. The elimination of intragrain pores, even if they are submicron in size, is a difficult and longer process than the elimination of closed interbrain pores. Intergrain pores are located at grain boundaries, acting as sinks of vacancies, which can be easily removed compared with those at other locations.

Ceramics consist of grains and grain boundaries. If there is a difference in properties, e.g., composition, between grains and grain boundaries, the interfaces between them will become scattering sites of light. To be transparent, the difference in optical behaviors between grains and grain boundaries should be minimized. Transparent ceramics have less clear grain boundaries, while opaque ceramics have clear grain boundaries. The presence of a second phase at the grain boundaries is generally the most common reason. Therefore, to fabricate transparent ceramics, it is necessary to use raw material of high purity and avoid any possible contamination during processing. Besides, care should be taken when selecting additives. For example, the amount of additives must be as low as possible, so that they completely dissolve in the solid solution with the main phase, without the presence of second phases.

Crystal structure plays an important role in determining whether ceramics can be optically transparent or not. In ceramics of optically anisotropic crystals, additional scattering of light arises at the boundaries when the light travels from one grain to another. This is the reason why transparent ceramics generally have a cubic lattice structure, which is isotropic, such as MgO, Y_2O_3, YAG ($Y_3Al_5O_{12}$), and $MgAl_2O_4$ (spinel) [4–6]. However, several materials that are not cubic crystal have also been made to be transparent, such as mullite, Al_2O_3 and some ferroelectrics. This means that the principles governing transparency of ceramics should be further studied. In fact, since the explanation was first proposed, it has never been challenged. For example, the first point is grain boundary. It is well known that ceramics always have grain boundaries. Therefore, this point should be revised to be quality of grain boundary, which means that grain boundaries cannot be avoided in ceramics, but the quality of grain boundary affects transparency.

Besides the internal factors, there are also external factors that affect transparency of a ceramic sample, including thickness and surface finish. A rough surface means a significant diffuse scattering, so the sample should be as smooth as possible. Generally, transparency decreases with increasing thickness. Thickness-independent transparency is only possible when the material reaches its theoretical maximum of in-line transmission.

In summary, the key strategy to develop transparent ceramics is to eliminate all possible scattering sites of light, including least porosity (>99.9 % of theoretical density), absence of pores at grain boundaries or pores with size smaller than the wavelength of light, absence of second phase (impurity or glass phase) at grain boundaries (negligible difference in optical property between grains and grain boundaries), high quality grain boundaries, small grain size (as compared to the

wavelength of visible light) with uniform size distribution, isotropic lattice structure, and high surface finish.

1.3 Important Issues on Transparency Important

Various transparent ceramics have been developed using different sintering techniques, combined with the use of ultrafine precursor powders with high sinterability. Although significant progress has been made on the one hand, there are certain problems in research in this area, of which a detailed discussion is presented in Ref. [7].

It is necessary to emphasize that a transparent component means that when it is used as a window a clear image of subjects far away from it can be formed. The prerequisite of such a clear image is the absence of any scattering when the light travels through the transparent window. Qualitative evidence by observation is used to show the transparency of transparent ceramics. The right way to do this is to maintain a sufficiently large distance between the objects and the transparent samples, as shown in Fig. 1.2a. In this way, it is clearly demonstrated that the Al_2O_3

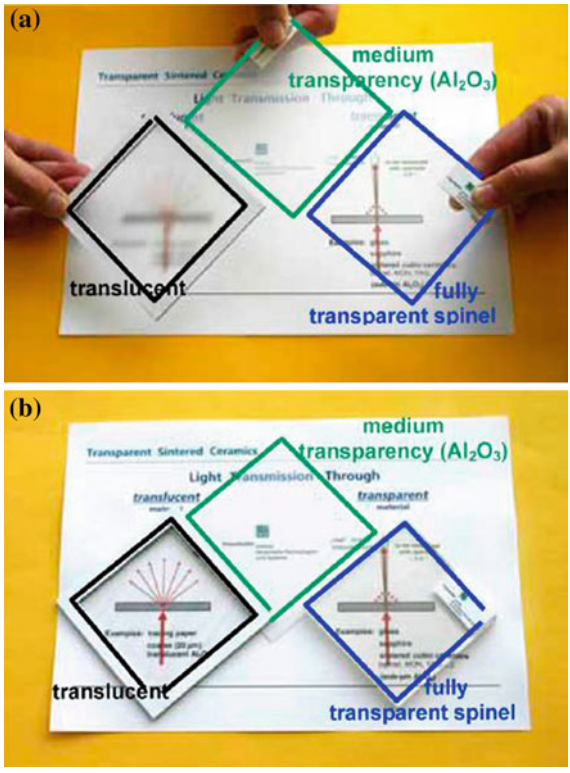

Fig. 1.2 Photographs of a thin translucent organic material of 0.06 mm, a sintered window of sub-μm Al_2O_3 (thickness 0.8 mm, real in-line transmission ~60 %) and 6 mm thick almost fully transparent spinel for comparison. The characteristic difference in transmission among the three samples is clearly demonstrated in **a**, while there is no clear difference due to the wrong positioning in **b**. Reproduced with permission from [7]. Copyright © 2009, Elsevier

sheet is translucent, while the spinel and organic samples are transparent. However, more generally, samples have been laid on background with a direct contact, as shown in Fig. 1.2b. In this case, all samples look like transparent. Another concern with accurate presentation of transparency is measurement. The apertures of most commonly used photospectrometers are in the range of 3°–5°, with which the measured transparencies are usually overestimated by including a fairly large amount of the scattered portion. For example, as the opening angle is increased from 0.5° to 5°, the recording area is increased by 100 times. Therefore, it is urgent to establish an international standard for the measurement of transparency of transparent ceramics.

Another important aspect is the so-called thickness effect if transparency of a material is below the theoretical maximum. As shown in Fig. 1.3a, b, the sample has 60 % of its theoretical transparency. As the sample thickness is increased from (b) to (a), the amount of scattered light is greatly increased. In other words, the real in-line transparency of the sample is reduced with increasing thickness. To exclude the contribution of scattered light, a narrow aperture should be used. Otherwise, the measured transparency will be overestimated. Only when a material reaches its theoretical maximum transparency, its transparency is not affected by thickness, as shown in Fig. 1.3c. In this respect, it is always desired to fabricate transparent ceramics with maximum transparency without any scattering or absorption. This is especially important for applications, such as armors, where a relative large thickness is necessary to ensure sufficiently high ballistic strengths.

As discussed earlier, various scattering losses are the main contribution to the decrease in in-line transmission, with respect to the theoretical maximum, of transparent ceramics, as summarized in Fig. 1.4 [7, 8]. Without the presence of these losses, the theoretical maximum of transmission is 100 % minus the reflection

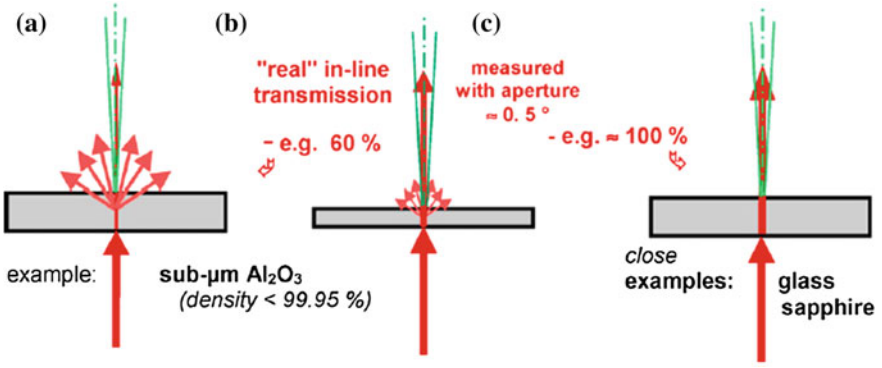

Fig. 1.3 Thickness effect (**b** → **a**) on in-line transmission of transparent of the transparent ceramics with an in-line transmission of <100 %, due to the scattering and/or absorption. "Real" in-line transmission is measured by using narrow measuring aperture (**b**). This thickness effect is absent as the transmission approaches the theoretical maximum (**c**). Reproduced with permission from [7]. Copyright © 2009, Elsevier

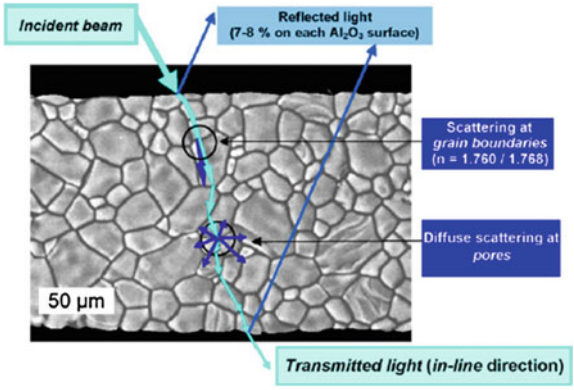

Fig. 1.4 Light transmission through polycrystalline translucent ceramics (e.g. coarse Al_2O_3). Loss in intensity of the incident light due to absorption, reflection on the two surfaces, diffuse scattering at pores and scattering caused by the birefringent splitting (specifically for noncubic materials). Reproduced with permission from [7]. Copyright © 2009, Elsevier

on both surfaces of a piece of the material. At normal incidence, the reflection R_1 on one surface is related to the material refractive index n, given as:

$$R_1 = \left(\frac{n-1}{n+1}\right)^2, \tag{1.1}$$

and the total reflection loss, including multiple reflection, is

$$R_2 = \frac{2R_1}{1+R_1}. \tag{1.2}$$

Therefore, the maximum transmission is as follows:

$$T_{\text{th}} = 1 - R_2 = \frac{2n}{n^2+1}. \tag{1.3}$$

When all the factors are present, the real in-line transmission (RIT) of a fully dense transparent ceramics can be described by the following equation:

$$\text{RIT} = T_{\text{th}} \exp\left[-3\pi^2\left(\frac{\Delta n}{n}\right)^2 \frac{rd}{\lambda^2}\right], \tag{1.4}$$

where $\Delta n/n$ is the ratio of refractive index difference between polarization perpendicular and parallel to c-axis to the average index n, $2r$ is grain size of the ceramics, λ is the wavelength of incident light, and d is thickness of the sample. This equation implies that, at a given thickness, the RIT is closely related to the $\Delta n/n$ and r. The smaller the values of $\Delta n/n$ and r, the high the RIT will be. If $\Delta n/n$ is an intrinsic

property of the materials, r is an extrinsic parameter that can be controlled through material processing. Therefore, for the given materials, the grain size of ceramics should be sufficiently small to achieve high RIT. For example, the grain size of a highly dense sintered Al_2O_3 has to be about 0.5 μm for RIT of 60–65 % at $\lambda = 640$ nm and $d = 1$ mm [7].

Besides, according to the definition of T_{th}, the transmission of transparent ceramics can never be 100 %. It is also necessary to mention that T_{th} in Eqs. (1.3) and (1.4) is calculated by assuming that the reflection occurs on a theoretically perfect surface. Because theoretically perfect surface is an ideal assumption, real ceramics inevitably have a certain value of roughness. Therefore, technical roughness gives rise to additional loss—another mechanism which decreases the real in-line transmission of products depending on the quality of surface preparation [7].

Traditional high-tech ceramics (e.g., for hip implants or cutting tools) are regarded as dense when their relative density reaches, e.g., 99.7 %. However, the starting point of increase in real in-line transmission is usually at residual porosities of <0.1–0.2 %. The key technology to achieve highly transparent ceramics is the use of high sintering temperatures (>1700 °C), even in cases when sintering facilities (HP, HIP or SPS) are used. As a result, transparent ceramics often have extremely large grain sizes (50–300 μm), which is detrimental to mechanical properties. In this light, development of transparent ceramics with fine-grain microstructure remains a challenge to the research community. Systematic knowledge of the relationship among the properties of precursor powders, green body preparation, as well as the combined use of various technologies, will be useful to address this problem, which is currently still lacking and thus deserves to be a subject of future research in this area.

1.4 History of Solid-State Lasers

1.4.1 Lasers

Lasers have been the main component in the optical range of quantum electronics, science of generation and amplification, control of properties, such as wavelength, temporal regime and power range, of radiation by the processes of interaction of electromagnetic radiation with quantum systems. The word LASER is an acronym, for light amplification by stimulated emission of radiation. The driving mechanism that determines the amplification of radiation in a laser is the stimulated emission in an ensemble of identical quantum systems, i.e., the active medium, with inversion of populations between a high energy level and a lower energy level, which act as emitting and terminal energy levels for the emission, in a resonator that provides the necessary conditions for amplification and extraction of the amplified radiation beam.

To discuss solid-state lasers, it is necessary to start with lasers in general. Laser was invented in the 1960s and has been growing quickly, with a wide range of applications in industry, defense, and daily life [2, 9–11]. According the properties of the gain medium used, lasers can be classified into four types: (i) semiconductor lasers, (ii) gas lasers, (iii) liquid (dye) lasers, and (iv) solid-state lasers.

Semiconductor lasers are mainly used as optical sources in optical communications and information storages. Gas lasers are optical sources usually used for measurements (He–Ne lasers), etching or lithography (Excimer) and industrial cutting, welding, or consolidating (CO_2 lasers). Dye lasers are highly tunable and can produce pulses of very short duration (of the order of femtosecond). Solid-state lasers represent a new class of lasers, including glass lasers and crystal lasers. Glass lasers are used in nuclear fusion reactors, while single crystal or ceramic (e.g., YAG) lasers have found applications in mechanical processing and medical equipment.

Various materials have been developed for solid-state lasers [12]. Crystalline solid-state laser materials include garnets, such as $Y_3Al_5O_{12}$ (YAG), $Gd_3Ga_5O_{12}$ (GGG), $Gd_3Sc_2Ga_3O_{12}$ (GSGG), and $Y_3Sc_2Ga_3O_{12}$ (YSGG) [13–16], fluorides such as CaF_2 and MgF_2 [17, 18], alexandrites [19–21] and other oxide-based materials [22–24], which can be either single crystals or polycrystalline ceramics. Noncrystalline materials are mainly silicate and phosphate glasses, containing Er, Yb, or Ce [25–28]. Physical properties of materials for solid-state lasers include high thermal conductivity, high chemical stability, and high mechanical strength. In terms of optical properties, they must have a large cross-section of stimulated emission (σ), long fluorescence lifetime (τ), low possible laser thresholds, and stable laser oscillation in continuous wave (CW). The best candidate is YAG, because it meets almost all the requirements.

Single crystals appeared earlier than ceramics for solid-state lasers. Melt-growth processes are used for single crystals. The Verneuil process is among the early single crystal growth techniques, also known as flame fusion process. Single crystals prepared using this method encountered quality problems in terms of laser performances. Currently, the most widely used single crystal growth technique is the Czochralski (Cz) process. It is well known that single crystal growth is very time-consuming. Usually, only limited portions of a single crystal have optical homogeneity for laser oscillations, because of the intrinsic core and facets that are determined by the growth characteristics. As a result, fabricated solid-state single crystal lasers are costly for large-scale applications.

Comparatively, the use of transparent ceramics could address these technical problems. However, due to the presence of grain boundaries, ceramic solid-state lasers have a common problem, i.e., the efficient amplification of the coherence beam in the materials could be disturbed. This problem was serious during the early state of ceramic solid-state lasers, such as Dy:CaF_2 and Nd:ThO_2–Y_2O_3. Although laser oscillation was observed by using these ceramics, the resulting beam quality and lasing efficiency were not sufficient for practical applications. However, the success of Nd:YAG ceramic laser revived ceramic solid-state laser. More importantly, ceramic materials can now exhibit equivalent laser performance of single

crystals. Therefore, the demonstration of Nd:YAG ceramic laser is a great milestone in ceramic solid-state lasers. This is because ceramic processing is significantly simpler than single crystals. It is believed that transparent ceramics will be dominant candidates for solid-state lasers in the future.

1.4.2 Single Crystals

In general, the performance of melt-growth technologies, such as homogeneity, uniformity, crystal size, doping concentration, productivity, and so on, are largely determined by thermophysical properties of the material, like melting temperature and thermal conductivity, thermochemical or thermostructural properties, and compositional limitation. On the other hand, growth equipment, including size of the crucible, thermal field distribution, mechanical stability, and so on, also plays an important role in determining the quality of the grown crystals.

The dominant single crystal for solid-state lasers is YAG, which is produced using the Cz melt-growth process [29]. Transition metal elements or lanthanide rare earth elements are used as laser active ions that are doped in YAG host material. Due to its narrow spectral width and high quantum efficiency, Nd ion, a four-level laser system has been acknowledged to be the most popular active ion.

Nd^{3+} ion has three fluorescent emissions: (i) 0.9 μm ($^4F_{3/2} \rightarrow {}^4I_{9/2}$), (ii) 1.06 μm ($^4F_{3/2} \rightarrow {}^4I_{11/2}$), and (iii) 1.3 μm ($^4F_{3/2} \rightarrow {}^4I_{13/2}$), with radiative transition possibilities of 0.25, 0.60, and 0.15, respectively [30–32]. Energy efficiency emission (ii) is the highest, so that Nd:YAG crystals are used for 1.06 μm generation. To achieve laser action in Nd:YAG, the electrons of Nd ions at the ground state are first excited with a xenon (Xe) or krypton (Kr) lamp, i.e., white light source from a discharge lamp, so that the electrons are pumped up to energy levels higher than $^4F_{3/2}$. Semiconductor lasers (LD, laser diode) of a certain wavelength can also be used to pump ground state electrons to the $^4F_{5/2}$ band. The excited electrons at the upper levels would decay rapidly to the $^4F_{3/2}$ level, which is a non-radiative transition. When these electrons are transferred to $^4F_{13/2}$, $^4F_{11/2,}$ and $^4F_{9/2}$, three fluorescent emissions, radiative transitions with $\lambda = 0.9$, 1.06, and 1.3 μm are obtained. As fluorescent emission is amplified by using a set of mirrors as resonator, an intensified light with a single wavelength, i.e., monochromatic light, is finally emitted.

When exciting with lamp source, electron transitions from the upper levels to the $^4F_{3/2}$ level are non-radiative and energy is released in the form of heat. As a result, effective laser oscillation cannot be obtained by using a system of lamp excitation. However, lamp excitation systems can offer high output powers, because lamps can supply very high input powers. If LD excitations are used, laser diodes of wavelengths 808 and 885 nm would pump the ground state electrons directly to upper levels, $^4F_{5/2}$ and $^4H_{3/2}$ levels, respectively. Because there are no excited electrons for non-radiative transitions in this case, efficient laser oscillation can be obtained. The only problem is that it was difficult to have high power LDs.

As stated earlier, YAG single crystals are grown using the Cz method. High purity starting materials, i.e., over 4N or 99.99 %, Y_2O_3, Al_2O_3 and Nd_2O_3 powders, have to be used to grow high purity single crystals. The powders were first mixed according to the stoichiometric composition of Nd:YAG. They were then pressed into pellets and sintered at certain temperatures. The sintered Nd:YAG pellets were put in an iridium (Ir) crucible and then melted through high frequency induction heating to a temperature of over 1950 °C. On the top surface of the YAG melt, a YAG seed crystal was positioned, which was then continuously pulled at very slow rates, e.g., 0.2 mm h^{-1} and rotated at speeds of 10–30 rpm. Because of large surface energy, the YAG seed crystals used have an orientation of ⟨111⟩. Of course, seeds with ⟨110⟩ and ⟨100⟩ orientations can also be used.

In YAG crystals, Nd^{3+} substitutes for Y^{3+}. Since the ionic radius of Nd^{3+} is larger than that of Y^{3+}, the segregation coefficient of Nd^{3+} in YAG, defined as the ratio of Nd concentration in the crystal to that in the melt, is as low as ~ 0.2 [11]. To grow an Nd:YAG crystal with desired concentration of Nd, it is necessary to use a precursor melt with 2–3 times higher Nd concentrations. In other words, 2–3 at.% Nd:YAG pellets have to be used to grow a 1 at.% Nd:YAG crystal. It has been found that inhomogeneous distribution of Nd is a bid problem of Nd:YAG single crystals. This is the reason why only Nd:YAG single crystals with Nd concentrations of ≤1 at.% are available for laser applications. Although at such low concentration, inhomogeneity is occasionally observed in parts, like the core and the (211) facets, which should be avoided when the crystals are used to make laser devices [11]. It is also observed that the as-grown Nd:YAG crystals often have a slightly gradient concentration of Nd in the longitudinal direction, simply because the concentration of Nd in the melt is increased gradually when the crystal becomes bigger and bigger, which forms another type of inhomogeneity.

In addition, the facilities as well as the Ir crucibles used for the growth of YAG crystals are extremely expensive. Also, due to slow growth rate, it usually takes months for one round of growth. Therefore, the growth process is energy-consuming. Furthermore, the yield percentage of high quality crystal is very low. All these disadvantages are intrinsic to melt-growth technologies [1, 11, 33]. To address these problems, it is necessary to use new processing, i.e., ceramic process.

1.4.3 Transparent Ceramics

The development of transparent ceramics is not so straightforward. Prior to the presence of transparent ceramics, translucent ceramics (Al_2O_3) were first reported [34]. However, these translucent ceramics could not be used for laser applications that require high optical quality, whereas they only found applications in the forms of thin layers, such as discharge tubes in high-pressure sodium vapor lamps. It was once believed that polycrystalline ceramics should be always opaque, i.e., ceramics could never be transparent. In this regard, the discovery of translucent Al_2O_3 ceramics was an encouraging event, because it demonstrated that light can transmit

through ceramics, as the bulk density of a ceramic is very close to its theoretical density.

Another exciting achievement is the development of Nd doped 10 % ThO_2–Y_2O_3 transparent ceramics, which enabled the production of laser oscillation at room temperature. That was the first polycrystalline ceramic gain medium for laser applications. Nd:ThO_2–Y_2O_3 transparent ceramics were prepared by sintering Y_2O_3 powder at high temperature of 2200 °C for a prolonged duration of about 100 h, with 10 % ThO_2 used as sintering aid [35–37]. Although pulse laser oscillation could be obtained by flashlamp excitation at room temperature, the performance was not sufficient for practical applications, e.g., the slope efficiency was only 0.1 %. The research on transparent ceramics has flourished since the discovery of transparent Nd:YAG ceramics.

For laser applications, because light amplification takes place in the gain medium and the amplified light travels through the gain medium repeatedly, even an optical loss would have a significant effect on laser oscillation. Optical loss is also called optical attenuation coefficient, which is used to quantitatively characterize the quality of transparent materials. The optical loss of high quality commercial single crystals is in the range of 0.3–0.2 % cm^{-1}, which can offer efficient laser generation. Comparatively, transparent ceramics have higher optical losses. This means that the optical quality of transparent ceramics should be further improved.

Till date, various transparent ceramics with high purity and high density have been produced, including simple oxides such as MgO, Y_2O_3, and ZnO, composite or complex oxides such as ZrO_2–Y_2O_3, YAG, spinel ($MgAl_2O_4$), ferroelectric PLZT ((PbLa)(ZrTi)O_3), SBN ($Sr_xBa_{1-x}Nb_2O_6$), Gd_2O_2S:Pr, and (YGd)O_3:Eu and even non-oxides such as AlON and AlN, for applications in solid-state laser, electro-optical devices, X-ray scintillators, and thermally conductive components, have been developed and/or commercialized [38–42]. Figure 1.5 shows a photograph of a high quality 1.0 at% Nd:YAG ceramic disk fabricated with optimized processing conditions [43].

The main strategies to ensure high optical quality of transparent ceramics include controlling the purity, particle size, and homogeneity of the precursor materials, exploring and understanding the sintering mechanisms of different materials, and the use of advanced sintering techniques.

Ceramic processing typically consists of three main steps: (i) synthesis or preparation of precursor powders, (ii) consolidation or packing of the powders into green bodies, and (iii) sintering [44]. Every step has a significant effect on the microstructure and optical performance of the final transparent ceramics. There are a number of parameters relevant to the quality of the powders, facility, and way of consolidation and techniques of sintering, which can be used to optimize the fabrication process as a whole.

Precursor powders of ceramics can be prepared using solids, such as oxides, hydroxides, and carbonates, as starting materials [45–50]. In this case, it is called the solid-state reaction process. The precursor powders can also be synthesized by wet-chemical methods, such as chemical precipitation or co-precipitation [51–59], sol–gel [60, 61], gel combustion [62–65] and hydrothermal synthesis [66–69]. The

solid-state powders react at a certain temperature to form compounds with desired compositions together with dopants, which is called calcination or pre-sintering. If the reaction is difficult, this step can be repeated. This step cannot be skipped even though no reaction is involved, e.g., the fabrication of simple oxide transparent ceramics. If a relative low calcination temperature is used, the reaction of the starting components cannot be triggered. In this case, the reaction will take place during the sintering process, so that the process is called reactive sintering. The products of chemical processes also need to have thermal treatment. For example, chemical precipitation usually yields carbides or hydroxides, which are decomposed into oxides by releasing water molecules or carbon dioxide. All the remaining steps are the same for the solid-state reaction process and the wet-chemical process.

These two methods have their own advantages and disadvantages. Solid-state reaction method is simple and can be easily scaled-up and thus is suitable for large-scale industrial applications. However, it has encountered various problems, including poor homogeneity in distribution of dopants and sintering aids, high sintering temperature, long sintering time duration, as well as poor microstructure and optical performance. Chemical procedures could have high homogeneity, fine powders, and thus low temperatures and short time duration. Their problems include complicated process, expensive chemicals, less quantity, and so on. Therefore, these methods are mainly used for fundamental studies of low quantity and small sizes in laboratories.

High doping of active components is an important requirement of transparent ceramics for laser applications. Homogeneous distribution of these elements in the final ceramics has a significant effect of laser performances. Also, when sintering aids are used to promote the sintering, their quantity should be restrictedly controlled, which must be as low as possible, in order to minimize their genitive effect on the optical properties of transparent ceramics. In this case, a combination of solid-state reaction and chemical processing can be used [70]. The main bodies of the materials are solids, while the additives (dopants and sintering aids) are introduced through wet-chemical routes. This is because chemical routes allow more homogeneous mixing.

It has been proved that the application of cold isostatic compression (CIP) before sintering is a crucial step to further increase the density of pre-sintered items, even though the increase in density is just in the range of 5–10 % [2, 9]. Special sintering techniques that are used to obtain high quality transparent ceramics include vacuum sintering, high-pressing (HP) sintering, hot isostatic pressure (HIP) sintering, as well as newly emerged spark plasma sintering (SPS), and microwave sintering. Specifically, SPS and HIP can be used to sinter transparent ceramics, with restrained grain growth [71–77]. This is especially important when mechanical strength is required for some applications.

1.5 Performance of Solid-State Lasers

A set of parameters, including efficiency, extension of wavelength range, diversification of temporal regime, power or energy scaling, and so on, are used to evaluate the performance of solid-state lasers [11]. The flow of excitation inside pumped laser materials should be optimized, so that there is a concurrent response of all the three major parts of a laser, i.e., the laser material, the pumping system, and the laser resonator. Good thermal management should be maintained, which determines the scaling to higher power or energy. This effect is caused by heat generation due to non-radiative de-excitation. The laser emission should be maximized while the heat generation should be minimized. Detailed discussion can be found in Ref. [11], a brief description will be given to each subject as follows.

1.5.1 Laser Materials

The core components of solid-state lasers are laser materials that allow for the inversion of population and amplification of radiation through stimulated emission. The properties of the laser materials determine the ways to design pumping system and laser resonator of a solid-state laser. Because the characteristics of laser active centers are determined by the physical processes related to the laser materials, while there are various possible interactions between the active centers and the electromagnetic radiations, the interrelationship among the composition, structure, properties, and functionality of laser materials is very complicated, leading the research in this field to be unlimited.

Similar to most advanced engineering materials, transparent ceramic laser materials also have various requirements for practical applications. The fabrication and processing process should be reliable, consistent, feasible, reproducible, energy saving, cost-effective, and scalable. More importantly, the compositions, both the main components and the dopants, must be under good control.

Optical properties of transparent ceramics are the first and foremost requirement for laser applications. For instance, they must be highly optically transparent in the spectral regions in order for pumping process and laser emission. Other optical properties include high optical homogeneity, minimized second-order refractive index, and high temperature stability in refractive index. Chemical stability and mechanical rigidity of the transparent ceramics are required to ensure the stability and lifetime of solid-state lasers. Thermophysical properties are also concerned in terms of stable laser performances, such as low thermal expansion coefficient, high thermal conductivity, strong thermomechanical shock-resistant capability, and acceptable temperature dependence of material properties.

The materials should meet specific requirements in compositions at microscopic levels. The substitution sites of low symmetry should be specific and well-defined in monochromatic lasers, while inhomogeneous broadening of lines are preferred in

tunable or ultrashort pulse lasers. In addition, the doping ions should preferentially have the same valences as the substituted ions, which is called charge balance requirement. Otherwise, charge compensation should be considered during processing of the materials.

The performances of laser materials have a close relation to their spectroscopic properties [11]. The combination of doping ions and host materials must provide electronic energy levels and transition probabilities to support the efficient laser emission schemes in the desired temporal regime: (i) strong absorption of the pump radiation and the possibility of controlling the pump rate distribution at pump wavelengths that allow a high quantum defect (Stokes) ratio $\eta_{\mathrm{qd}}^{(l)}$, (ii) efficient de-excitation of the pump level to the emitting level, i.e., $\eta_{\mathrm{p}} \approx 1$, (iii) long radiative lifetime τ_{rad} of the emitting level, (iv) negligible electron–phonon de-excitation W_{nr} of the emitting level, but very efficient de-excitation of the pump level to the emitting level and the terminal level to the ground state, (v) reduced self-quenching by downconversion or upconversion energy transfer and high emission quantum efficiency η_{qe}, to give long τ_{eff}; (vi) emission cross-section σ_{e} adapted to the temporal regime, (vii) reduced parasitic de-excitation by excited state absorption from the emitting level of the pump or laser emission, and (viii) reduced reabsorption of laser emission.

1.5.2 Pumping Systems and Laser Resonators

Regarding pumping systems, the emission spectrum should have promising superposition of absorption for laser materials, in order to minimize the content of quantum defects. Also, the pumping systems should have desired temporal regime for the continuous wave or pulsed wave, high power output, long life span and stable emission characteristic, high electrical–optical efficiency, high transfer efficiency, and so on.

Laser resonators should have appropriate laser transition, good control of outcoupling, high quality factor to ensure the desired temporal regime of emission, control of the mode structure and beam size, control of the thermal field (dissipation of heat, external cooling). Technical requirements include mechanical robustness, volumetric compact, lowest maintenance, and simple replacement of parts/components.

1.6 Selection of Laser Material

Laser performances are determined by the properties of laser materials. Therefore, the selection of laser materials is an important step in building a high performance solid-state laser. The absorption and emission properties of the doping ions should

be appropriate for lasing requirements, whereas the host materials should have required optical, mechanical, and thermal properties.

1.6.1 Laser Active Ions

Laser active ions are those that have energy level structures and transition probabilities, thus limiting to those with ground configuration of $3d^n$ or $4f^n$. In other words, laser active ions are from transitional elements.

1.6.1.1 3d Ions

The 3d ions for laser applications include Ti^{3+}, Cr^{n+} ($n = 2, 3, 4$) $V^{3+,}$ and Co^{2+}. Ti^{3+}-doped Al_2O_3 crystal (sapphire) belongs to the family of vibronic laser materials, which are the most promising candidates for tunable or short pulse laser emissions. The Ti^{3+}-doped Al_2O_3 system offers tunable emission at about 800 nm, covering a range of about 230 nm, with femtosecond pulses. Lasers with peak powers of petawatts have been available in chirped pulse amplification (CPA) systems based on Ti:sapphire systems. Due to the difficulties in pumping and making large size sapphire crystals, this type of laser has limited applications.

With promising absorption and emission properties, Cr^{n+} ions with different valences ($n = 2, 3, 4$) can be used as either laser active ions or sensitizers for weakly absorbing 4f ions. Cr^{4+} ion tends to occupy sites with tetrahedral coordination, which has strong absorption in the range of wavelength from visible to 1 μm, with σ_a of $3.5–7.0 \times 10^{-18}$ cm^2. The ion has infrared emission over 1350–1580 nm, with a high intensity σ_e of $3–5 \times 10^{-19}$ cm^2, short lifetime of microseconds, and a broad range of >200 nm, depending on host materials. Cr^{3+} ion prefers to take six-fold coordinated sites, which can have broad vibronic emission lines near infrared when the excited level $^4T_2$ is below the ^2E level, because there is a strong spin-allowed emission to the ground $^4A_2$ level. Also, since it can be sufficiently thermalized, a relatively long effective emission lifetime is available, which is 60–100 μs. Additionally, due to strong vibronic absorption lines in visible region, Cr^{3+} ion can be used for direct lamp or diode laser pumping. At tetrahedral coordination sites, Cr^{2+} ion has a strong broad absorption centered at about 1750 nm and a short strong broad emission centered at about 2450 nm, which are corresponding to the vibronic transitions between $^5T_2$ and ^5E.

V^{3+} ion at octahedral coordination sites exhibit strong absorption over 1.05–1.5 μm, with an absorption cross-section of $\sim 1.3 \times 10^{-18}$ cm^2, which can be used for *Q*-switching of 1.3 μm lasers. Similarly, Co^{2+} ion at weak field tetrahedral coordination sites can also be used for *Q*-switching of 1.3 μm lasers.

1.6.1.2 4f Ions

Due to their wide range of sharp fluorescent transitions, which cover almost the whole region from the visible and near-infrared portions of the electromagnetic spectrum, all the rare earth (RE) ions are promising candidates as active ions in solid-state lasers. More significantly, it is found that all these lines are sufficiently sharp for strong lasing applications, even though strong local fields of crystals are present, due to the shielding effects of the outer electrons.

Rare earth atoms are characterized with a ground-state electronic configuration, which consists of a core that is identical to that of xenon (Xe), while the remaining electrons occupy higher orbital levels. The shells of Xe atom, with quantum numbers $n = 1$, 2, and 3 are completely filled, while in the shell with $n = 4$, s, p, and d subshells are fully filled, whereas the 4f subshell capable of accommodating up to 14 electrons is empty. However, in the shell of $n = 5$, the 5s and 5p orbits are fully filled with eight electrons.

The elements after Xe have this electronic configuration, plus electrons in the orbits of 4f, 5d, 6s, and so on. There are three elements, Cesium (Cs), barium (Ba), and lanthanum (La), between Xe and the RE elements. Cs has one 6s electron and Ba has two 6s electrons, while La has two 6s and one 5d electrons. When it comes to RE elements, the electrons start to fill the inner vacant 4f orbits. For instance, the first RE element Ce has only one electron in the f orbit, so that its configuration is $[Xe]6s^2 4f^1 5d^1$, while neodymium (Nd) has four electrons in the f orbit, i.e., its electron structure is $[Xe]6s^2 4f^4$.

RE ions are usually trivalent or occasionally divalent at a certain special environment. For RE^{3+} ions, outermost 6s electrons are all given up and the 5d electron is lost, if there is. If there is no 5d electron, one of the 4f electrons will be lost. For example, Ce^{3+} ion has an electronic configuration of $[Xe]4f^1$, while the electronic configuration of Nd^{3+} ion is $[Xe]4f^3$. Therefore, after becoming ions, the electronic configurations of the RE elements become simpler. As listed in Table 1.1, the RE ions are only different in the number of electrons in the 4f shell [78]. IF the RE elements are present as divalent ion, only the two outermost 6s electrons are lost.

Owing to the presence of potential electronic transitions between different levels of the partially filled 4f shell, RE ions offer a wealth of fluorescence spectra. Electrons in the 4f shell can be excited into the unoccupied 4f levels when absorbing light radiation. Because the 4f states are well shielded by the outer filled shells of 5s and 5p, the emission lines are usually narrow and the energy level structure varies only slightly for different host materials. According to crystal field theories, the effect of the crystal field is considered to be a perturbation on the energy levels of free ions. Comparatively, this perturbation is smaller than the spin-orbital and electrostatic interactions among the 4f electrons. The variation in the energy levels is a splitting of each of the free-ion levels into many closely spaced levels, which is known as the Stark effect of the crystal field. In this case, the levels of free ions are referred to as manifolds in crystals. All the RE^{3+} ions, except Yb^{3+}, exhibit a pretty complex energy level structure, so that there are laser emissions on several inter-manifold transitions [11]. As an example, Fig. 1.6 shows the splitting

Table 1.1 Electronic configurations of trivalent rare earth (RE) elements [78]

Element No.	RE element	Trivalent ions	4f electrons	Ground state
58	Cerium	Ce^{3+}	1	$^2F_{5/2}$
58	Praseodymium	Pr^{3+}	2	$^3H_4$
60	Neodymium	Nd^{3+}	3	$^4I_{9/2}$
61	Promethium	Pm^{3+}	4	$^5I_4$
62	Samarium	Sm^{3+}	5	$^4H_{5/2}$
63	Europium	Eu^{3+}	6	$^7F_0$
64	Gadolinium	Gd^{3+}	7	$^8S_{7/2}$
65	Terbium	Tb^{3+}	8	$^7F_6$
66	Dysprosium	Dy^{3+}	9	$^6H_{15/2}$
67	Holmium	Ho^{3+}	10	$^5I_8$
68	Erbium	Er^{3+}	11	$^4I_{15/2}$
69	Thulium	Tm^{3+}	12	$^3H_6$
70	Ytterbium	Yb^{3+}	13	$^2F_{7/2}$
71	Lutetium	Lu^{3+}	14	$^1S_0$

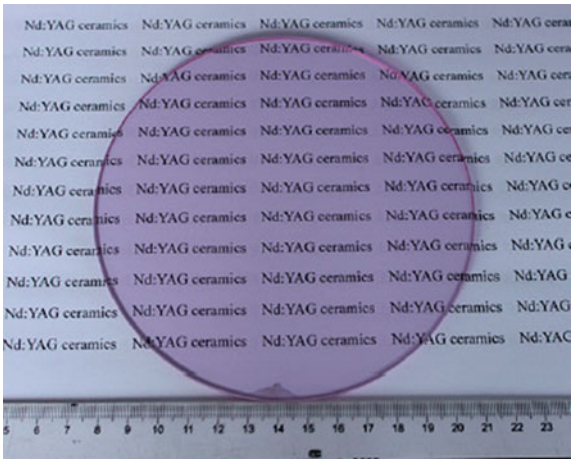

Fig. 1.5 Photograph of a high quality 1.0 at% Nd: YAG ceramic disk with a dimension of Ø130 mm × 6 mm. Reproduced with permission from [43]. Copyright © 2012, Elsevier

behavior of the Nd^{3+} manifolds into various sublevels, under the perturbation of the YAG crystal field [78].

Pr^{3+} Ion Due to the manifold $^3P_0$ located in the 20,500 cm^{-1} region, Pr^{3+} ion has been demonstrated to exhibit laser transitions in the visible, from blue, green, orange to red, as well as near-infrared region. The manifold $^3P_0$ has a large emission cross-section, especially for the red transition of $^3P_0 \rightarrow {}^3F_2$. Therefore, Pr^{3+} has been extensively studied as a laser active ion. However, Pr^{3+} ion has a relatively

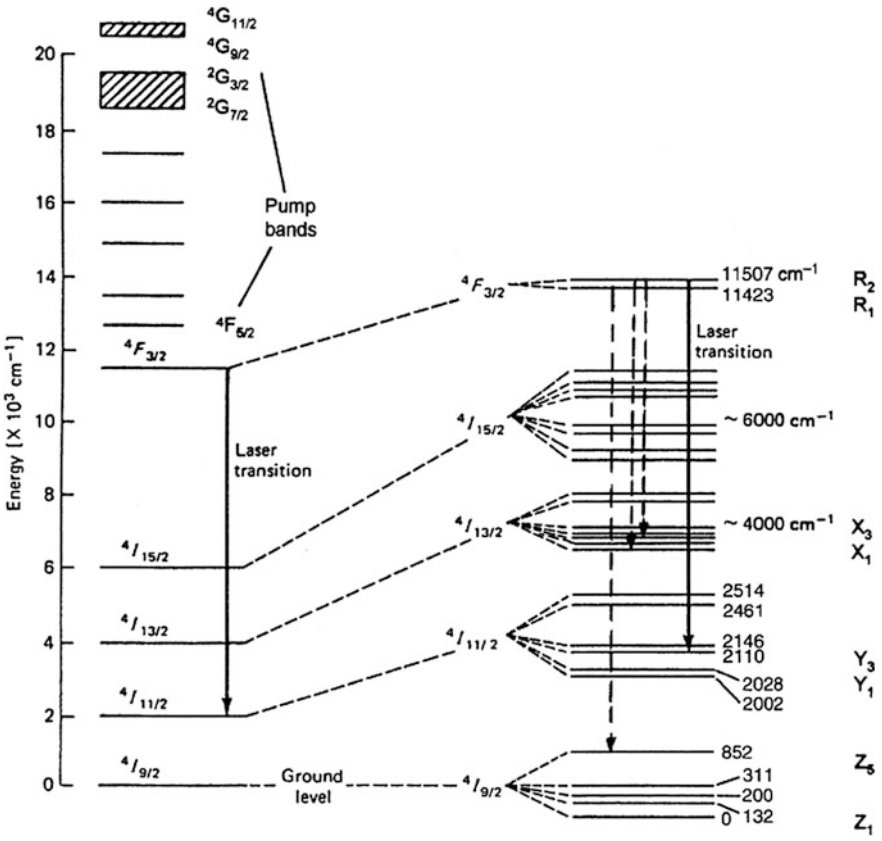

Fig. 1.6 Energy level diagram of Nd:YAG, in which the *solid line* represents the major transition at 1064 nm, while the dashed lines are transitions at 1319, 1338, and 946 nm. Reproduced with permission from [78]. Copyright © 2006, Springer

short lifetime, which is about tens of microseconds. The main problems of Pr^{3+} ion is the lack of suitable pump sources and the weak absorption.

Nd^{3+} Ion With a ground configuration of $4f^3$, Nd^{3+} ion has a complicated structure of energy manifolds. Among these manifolds, only that of $^4F_{3/2}$, at about 11,500 cm^{-1}, is in a metastable state. Depending on the host material that the ion is in, it has radiative lifetimes in the range of 80–500 μs. Below the metastable manifold, four manifolds are observed, which are ^4I_J, with $J = 9/2$, 11/2, 13/2, and 15/2. These manifolds stem from the same spectral term ^4I. The gap between $^4F_{3/2}$ and the one nearest it, $^4I_{15/2}$, is at about 5500 cm^{-1}. This gap has p of 7–10, which can be bridged only when very high order electron–phonon processes are present. If the concentrations of Nd are sufficiently low, the measured luminescence lifetime at temperatures can be used estimate the radiative lifetime. At low symmetry crystal field, each of these energy manifolds will be split into $(2J + 1)/2$ Kramers doublets,

which are labeled as R_i with $i = 1, 2$ for $^4F_{3/2}$, X_j with $j = 1$ to 7 for $^4I_{13/2}$, Y_j with $j = 1$–6 for $^4I_{11/2,}$ and Z_j with $j = 1$–5 for $^4I_{9/2}$. The global crystal field splitting behaviors of the manifolds in different host materials can be greatly different, which are in the ranges of 0–250 cm^{-1} for $^4F_{3/2}$, 400–1000 cm^{-1} for $^4I_{15/2}$, 240–690 cm^{-1} for $^4I_{13/2}$, 190–525 cm^{-1} for $^4I_{11/2,}$ and 280–880 cm^{-1} for $^4I_{9/2}$ [11].

Because laser emission of Nd^{3+} ion is attributed to optical transitions between the Stark levels of the emitting and terminal manifolds, it has $2j$ possible optical transitions between the two Stark levels of the emitting manifold $^4F_{3/2}$ and the Stark levels of lower manifolds. The effective lifetime τ_{eff} of all these transitions is the same, whereas their laser quantum defect ratio $\eta_{qd}^{(l)}$ and emission cross-section σ_e are different. Since temperature has an effect on the fractional thermal population coefficients $f_{1,2}$ of the levels $R_{1,2}$ of $^4F_{3/2}$, the effective emission cross-sections σ_{eff} and laser threshold are also dependent on temperature. The slope efficiency $\eta_{sl}^{(a)}$ of all the laser transitions is only determined by the particular quantum defect, which is also independent on temperature.

Many of the transitions in the range of near 900 nm to the ground manifold $^4I_{9/2}$ possess laser emission, while some of them have cross-sections of $>10^{-20}$ cm^2 at room temperature. The Judd–Ofelt parameters have been used to calculate the branching ratios β_{ij} of the emission transitions due to the excited manifold. For emission of $^4F_{3/2}$, the quality factor $X = \Omega_4/\Omega_6$ is particularly important. For very small values of X, the branching ratio $\beta_{3/2,11/2}$ is dominant, which is about 0.66 for $X = 0$ and is found to decrease with increasing X. In contrast, $\beta_{3/2,9/2}$ is relatively low, which is only about 0.17 for $X = 0$, but it increases with increasing X. As a result, there is a crossing point for these two branching ratios, which is about $X \approx 1.15$. The branching ratio $\beta_{3/2,13/2}$ decreases from 0.17 at $X = 0$ to less than 0.1 for $X = 2$, while $\beta_{3/2,15/2}$ is very small, which is usually negligible.

Due to the high density of the excited levels above the emitting level, excitations with a broad range of wavelengths in the visible and near-infrared region have been observed. Because all these excitations are relaxed to $^4F_{3/2}$ through a series of very fast processes, the pumping of Nd lasers can be achieved using various optical sources, e.g., lamps, solar, diode lasers, and so on.

Nd^{3+} ion has a disadvantage, which is called self-quenching of emission, due to its complex electronic structure. For downconversion, an excited Nd^{3+} ion in the $^4F_{3/2}$ level could transfer part of the excitation to an unexcited Nd^{3+} ion. At room temperature, the process is dominated by the cross-relaxation process, i.e., ($^4F_{3/2}$, $^4I_{9/2}$) → ($^4I_{15/2}$, $^4I_{15/2}$). In most Nd-doped laser materials, the final levels of the donor and acceptor are further de-excited to the ground state through efficient low order electron–phonon processes, so that the initial excitation of the donor ion is completely wasted as the form of heat. The interaction between two excited Nd^{3+} ions can induce upconversion of excitation to an upper level, through the cross-relaxation processes, ($^4F_{3/2}$, $^4F_{3/2}$) → one of ($^4I_{15/2}$, $^4G_{5/2}$), ($^4I_{13/2}$, $^4G_{7/2}$), ($^4I_{11/2}$, $^4G_{9/2}$) and ($^4I_{9/2}$, $^2P_{1/2}$). Due to the high density of the levels above $^4F_{3/2}$, all the excitation transferred to the acceptor will be lost through the electron–phonon

interaction, so that the excited acceptor returns to its initial excited level $^4F_{3/2}$. Therefore, downconversion is more wasteful than upconversion. Nevertheless, Nd^{3+} ion has been acknowledged to be one of the most popular laser active ions, due to its wide range of possibilities.

Ho^{3+} Ion Ho^{3+} has a ground electronic configuration of $4f^{10}$, with several well separated levels for emissions in the visible or infrared range. Among these emissions, the 2.1 μm one, i.e., $^5I_7 \rightarrow {}^5I_8$, is the most important, which has a cross-section of about 10^{-20} cm^2 and lifetime of about 7 ms. Because the visible and near-infrared absorption lines of Ho^{3+} are relatively weak, it is usually sensitized using either Tm^{3+} or Cr^{3+}–Tm^{3+}. It has also been demonstrated that efficient 2 μm laser emission with low quantum defect can be realized by pumping directly into the emitting level $^5I_7$ with a Tm^{3+} laser or diode lasers. Also, excitation of visible emission can be obtained through various upconversion schemes.

Er^{3+} Ion The ground configuration of Er^{3+} is $4f^{11}$, which offers a very rich electronic level structure. Several levels in the visible and near infrared are well separated to give emission. It exhibits accidental coincidence of the gaps between various pairs of energy levels, which facilitates a large variety of ET downconversion or upconversion processes. Some of the low energy levels, such as $^4I_{11/2}$ located at about 10,000 cm^{-1} and $^4I_{13/2}$ at about 6500 cm^{-1} have long radiative lifetimes of 6–9 ms. Efficient emission can be obtained on the four-level transition, $^4I_{11/2} \rightarrow {}^4I_{13/2}$, in the range of 2.7–2.95 μm. However, the luminescence lifetime of the terminal level is longer than that of the emitting level, which makes the laser emission to be rapidly self-saturated. This problem can be addressed by using high Er doping, because the migration-assisted ET upconversion, ($^4I_{13/2}$, $^4I_{13/2}$) $\rightarrow$ ($^4I_{9/2}$, $^4I_{15/2}$), can efficiently depopulate the level, so as to recirculate part of the excitation to the $^4I_{9/2}$ level, which could be relaxed back to the emitting level $^4I_{11/2}$. Another upconversion from the level $^4I_{11/2}$, through ($^4I_{11/2}$, $^4I_{11/2}$) $\rightarrow$ ($^4S_{3/2}$, $^4I_{15/2}$) could reduce the effect of that upconversion. Therefore, these two upconversion processes must be well balanced.

$^4I_{13/2} \rightarrow {}^4I_{15/2}$ is a quasi-three-level transition, with emission cross-section of about 5×10^{-21} cm^2, which can be used for laser emission in the range of 1.55–1.65 μm. This laser emission is eye-safe radiation, which can be used to replace the eye-dangerous 1 μm lasers. It also has potential application in telecommunications, due to matching with the range of minimal absorption of glass fibers. There are also transitions from high energy levels for Er^{3+} laser emissions in the visible region, especially green or red emission from $^4S_{3/2}$.

Weak pump absorption is a disadvantage of Er^{3+}, but this problem has now been addressed through co-doping with sensitizer ions. For instance, sensitization with Cr^{3+} has been used in lamp pumping. It is possible to excite the $^4I_{11/2}$ level using 960 nm diode lasers, whose low efficiency due to the low absorption has been addressed by using co-doping with Yb^{3+}, because Yb^{3+} has larger absorption and can transfer the excitation efficiently to Er^{3+}. It has been found that $^4I_{11/2}$ can be rapidly de-excited to $^4I_{13/2}$ by using the ET to other ions, such as Ce^{3+}, because the

absorption of Ce^{3+} is resonant with this energy gap. This can be used to improve the efficiency of excitation of the 1.6 μm $^4I_{13/2}$ emission with Er^{3+} through sensitized pumping. The upper energy levels for visible emission can be excited by ET upconversion and/or excited state absorption of the infrared pump radiation, while the energy transfer from Yb^{3+} can be used for sensitization of similar upconversion processes.

Tm^{3+} Ion Tm^{3+} has a ground configuration of $4f^{12}$, with well-separated levels that facilitate emissions in the visible and infrared range. Among them, the quasi-three-level emission in the range of 2 μm due to the transition from the first excited manifold $^3F_4$, located near 5000 cm^{-1}, to the ground level $^3H_6$, is the most important one. Tm^{3+} has strong electron–phonon interaction, thus leading to significant homogeneous broadening of the lines. The emission cross-section in this transition is relatively small, of the order of 10^{-21} cm^2, which is compensated by the long lifetime of level $^3F_4$, i.e., 8–10 ms. It is also found that the $^3F_4$ level can be efficiently populated through quantum splitting of the excitation of level $^3H_4$, located at about 12,500 cm^{-1}, via cross-relaxation, ($^3H_4$, $^3H_6$) → ($^3F_4$, $^3F_4$). Weak absorption is a major problem for pumping Tm^{3+} in the visible and infrared region, which can be sensitized by using 3d ions such as Cr^{3+} or Fe^{3+}. The visible emission from Tm^{3+} can be excited by upconversion processes, especially the Yb-sensitized upconversion.

Yb^{3+} Ion The ground electronic configuration of Yb^{3+} is $4f^{13}$, which has only two manifolds, $^2F_{7/2}$ at ground and $^2F_{5/2}$ in the region of 10,000 cm^{-1}. Such a configuration precludes emission self-quenching through cross-relaxation or excited state absorption. Because it is at the end of the lanthanide series, Yb^{3+} has strongest electron–phonon interaction and crystal field effects. As a result, Yb-doped materials have broad emission lines and strong vibronic satellites. The global crystal field splitting of $^2F_{5/2}$ with three Stark levels and $^2F_{7/2}$ with four Stark levels can reach 600 and 1200 cm^{-1}, respectively. The emission transitions are in the range 960–1060 nm. The lower Stark levels of $^2F_{7/2}$ can experience thermal population, which could result in strong reabsorption, thus limiting the useful range for laser emission to 1025–1060 nm. Compared with the emitting level $^4F_{3/2}$ of Nd^{3+}, the level $^2F_{5/2}$ of Yb^{3+} has longer lifetime, but lower absorption and smaller emission cross-sections.

The $^2F_{7/2}(1) \rightarrow {}^2F_{5/2}(1)$ absorption line in the range of 960–980 nm, with the highest peak absorption cross-section, is very sharp and exhibits strong homogeneous broadening. Therefore, diode pumping of this line requires restrictive control of the peak wavelength and FWHM of the pump. The broader $^2F_{7/2}(1) \rightarrow {}^2F_{5/2}(2)$ absorption line at about 940 nm is used for diode laser pumping, because its relatively small cross-section can be addressed by various techniques, such as fiber or thin-disk multi-pass laser configurations. Bulk Yb lasers require high doping concentrations. Reduction in thermal conductivity could be a problem of Yb^{3+} lasers, especially when the mass difference between the substituted ion and Yb^{3+} is

significantly large. In most Yb laser materials, the $^2F_{5/2}(1) \rightarrow {}^2F_{7/2}(3)$ emission line has the highest peak cross-section, but with reabsorption.

Yb laser materials have shown to be promising candidates for highly efficient and low-heat diode pumped laser emission in various regimes, due to their unique properties, such as large product $\sigma_{\text{eff}}\tau_{\text{eff}}$ to enable efficient CW emission, long τ_{eff} to ensure efficient storage of inversion for Q-switched emission, broad emission lines suitable for mode-locked short pulse emission, and so on.

1.6.2 Host Materials

Due to the special characteristics of the laser emission process and the parasitic non-radiative de-excitation, it is necessary to carefully select the laser materials, including both the active ions and host materials. In addition, the characteristics of dopants and the states of doping have also played a crucial role in determining the performances of laser materials and thus the solid-state lasers. The efficiency and effectiveness of doping is mainly determined by the degree of matching in ionic radii between the dopant ions and substituted cations. The Shannon ionic radii of the RE^{3+} ions in condensed state with anionic coordination number of 6 and 8 are r_6 = 0.103–0.115 nm and r_8 = 0.113–0.128 nm, respectively. In both cases, the radius decreases with increasing atomic number [79]. These ions can substitute for host cations with similar ionic radius, such as Ca^{2+}, Sr^{2+}, La^{3+}, Gd^{3+}, Y^{3+}, Lu^{3+}, $Sc^{3+,}$ and so on. The efficiency of the substitution is closely related to the conditions of fabrication and processing of the laser materials, such as properties of starting materials, synthesis methods, processing parameters, and so on.

It has been found that doping with laser active ions can greatly reduce the thermal conductivity of the host materials. Therefore, doping leads to an additional criterion for the selection of the host material, i.e., the atomic mass of the substituted cation should be as close as possible to that of the doping ion. The ionic radii of both the laser active ions and host cations have been well documented as database in the open literature. The doping efficiency is also related to valences of the doping and substituted ions. The difference in valence requires charge compensation, which is realized by creating lattice defects, such as vacancies or interstitials. Occasionally, heavy doping of ions with a significant valence difference could result in severe crystalline lattice restructuring or phase transformation.

There are also other requirements for the host materials, such as mechanical strength, chemical stability, fabrication processibility, and so on, which should be taken into account during the selection of host materials. All raw materials and procedures involved should be cost-effective, especially for large-scale production, otherwise no industry will adopt.

1.7 Other Applications of Transparent Ceramics

Besides the main application in solid-state lasers, transparent ceramics have also found various other applications, including lighting, scintillators, armors, optical devices, electro-optical devices, and biomaterials. While all these applications require high optical transmission, in some cases, high mechanical strengths are also important, for example, in armor applications. As stated earlier, mechanical strength is closely related to the grain size and size distribution of transparent ceramics. Reducing grain size is the key strategy to increase the mechanical performance of ceramic materials.

1.8 Motivation and Objectives of the Book

Due to their important applications in solid-state lasers and many other areas, transparent ceramics have attracted the attention of researchers from laser physics, applied physics, chemistry and materials science and engineering. However, ceramic lasers are a highly multidisciplinary or interdisciplinary subject, involving laser physics and materials processing at the same time. There are numerous books available in either solid-state layers [80–83] or ceramic processing [44, 84–86], but very few that cover evenly both fields [11, 87]. Therefore, the aim of this book is to bridge the gap between solid-state transparent ceramic lasers and transparence ceramic processing. At the same time, transparent ceramics for other applications will also be elaborated.

1.9 Outline of the Book

This book consists of eight chapters. Chapter 1 provides a brief introduction to transparent materials, transparent ceramics, issues on transparency of transparent materials, and solid-state lasers (including single crystals and ceramics). Requirements and availabilities of materials for solid-state lasers are also evaluated and discussed in detail.

In Chap. 2, materials that can be processed into ceramics for solid-state laser and related applications are elaborated, including brief descriptions on crystal structure, physical properties, phase formation, and processing requirements. The dominant transparent ceramics are still for solid-state laser applications. Among the laser ceramics, YAG-based ones are the most widely studied and described. With the development of new sintering technologies, especially SPS, various new transparent ceramics, which cannot be obtained using conventional processing techniques, have been fabricated. New transparent ceramics derived from glass precursors will also be touched upon in this chapter.

Chapter 3 covers synthesis of precursor powders of transparent ceramics. These synthetic methods are also widely used for other ceramics or other materials. For each method, a brief description, together with examples of transparent ceramics derived from the powder synthesized by using the method, will be presented. There is no attempt to comment on whether one method is superior to another. In fact, every method has its own advantages and disadvantages. Different methods could be suitable for different transparent ceramic materials.

Chapter 4 consists of two parts: (i) powder characterization and (ii) consolidation of ceramic powders. In the powder characterization part, efforts have been made to include as many techniques as possible, which have been used or are potentially useful to characterize the precursor powders of transparent ceramics. In the powder consolidation part, various packing techniques are discussed and demonstrated with examples of transparent ceramics.

Various conventional sintering techniques, such as vacuum sintering, high-pressure sintering, and high-isostatic pressure sintering, are discussed in Chap. 5, in terms of producing high quality advanced ceramics in general and transparent ceramics in particular. Fundamental issues regarding conventional sintering are re-emphasized, including driving forces of sintering, progress of sintering, and liquid-phase sintering.

New sintering technologies, mainly electrical current aided sintering (ECAS) and microwave sintering, are presented in Chap. 6, where ECAS is also known as SPS. Theoretical considerations, simulation, and applications of the two new sintering technologies are discussed first in a more general way, which is not restricted to transparent ceramics. For the theoretical and modeling part of SPS, not only the achievements on ceramics are described, but also some related contents of metallic materials are included as well for the purpose of completeness.

In Chap. 8, grain growth and microstructure development of ceramics as a result of sintering are presented. Besides general theoretical and experimental studies, some topics are specifically emphasized, such as abnormal grain growth (AGG) and two-step sintering. AGG is mainly used to convert polycrystalline ceramics into single crystals, which is also known as solid-state conversion of single crystal. Two-step sintering is employed to control grain size, which is of special importance for the transparent ceramics with the requirement of high mechanical strength.

Applications of transparent ceramics are covered in the last two chapters, with Chap. 9 focusing on solid-state lasers with transparent ceramics and Chap. 10 on all other applications of transparent ceramics. In Chap. 9, besides traditional transparent laser ceramics, advanced ceramic laser technologies, including composite ceramics and crystal fibers (not ceramics), are also included, in order to demonstrate new research and development direction of solid-state lasers. In Chap. 10, other applications, such as lighting, scintillation, armor, potential biomaterials, and so on, are summarized and discussed.

Although each chapter covers only a specific topic, all the chapters are compiled in such a way that each one is self-consistent, so as to be read as an independent monograph.

Acknowledgments One of the authors (LBK) would like to acknowledge the financial supports from the start-up grant (SUG/2012) from Nanyang Technological University and AcRF Tier 1 project (RG44/12) from Ministry of Education, Singapore.

References

1. Wang SF, Zhang J, Luo DW, Gu F, Tang DY, Dong ZL et al (2013) Transparent ceramics: processing, materials and applications. Prog Solid State Chem 41:20–54
2. Ikesue A, Kinoshita T, Kamata K, Yoshida K (1995) Fabrication and optical properties of high-performance polycrystalline Nd-YAG ceramics for solid-state lasers. J Am Ceram Soc 78:1033–1040
3. Ikesue A, Aung YL (2008) Ceramic laser materials. Nat Photonics 2:721–727
4. Sanghera J, Bayya S, Villalobos G, Kim W, Frantz J, Shaw B et al (2011) Transparent ceramics for high-energy laser systems. Opt Mater 33:511–518
5. Sanghera J, Kim W, Villalobos G, Shaw B, Baker C, Frantz J et al (2012) Ceramic laser materials. Materials 5:258–277
6. Sanghera J, Kim W, Villalobos G, Shaw B, Baker C, Frantz J et al (2013) Ceramic laser materials: past and present. Opt Mater 35:693–699
7. Krell A, Hutzler T, Klimke J (2009) Transmission physics and consequences for materials selection, manufacturing, and applications. J Eur Ceram Soc 29:207–221
8. Apetz R, van Bruggen MPB (2003) Transparent alumina: a light-scattering model. J Am Ceram Soc 86:480–486
9. Ikesue A, Kamata K, Yoshida K (1996) Synthesis of transparent Nd-doped HfO_2-Y_2O_3 ceramics using HIP. J Am Ceram Soc 79:359–364
10. Ikesue A, Kamata K (1996) Microstructure and optical properties of hot isostatically pressed Nd:YAC ceramics. J Am Ceram Soc 79:1927–1933
11. Ikesue A, Aung YL, Lupei V (2014) Ceramic lasers. Cambridge University Press, Cambridge
12. Maiman TH (1960) Optical and microwave-optical experiments in ruby. Phys Rev Lett 4:564–566
13. Drube J, Struve B, Huber G (1984) Tunable room-temperature CW laser action in Cr^{3+}-GdScAl-garnet. Opt Commun 50:45–48
14. Struve B, Huber G (1985) The effect of the crystal-field strength on the optical-spectra of Cr^{3+} in gallium garnet laser crystals. Appl Phys B Photophysics Laser Chem 36:195–201
15. Moulton PF, Manni JG, Rines GA (1988) Spectroscopic and laser characteristics of Er, Cr-YSGG. IEEE J Quantum Electron 24:960–973
16. Caird JA, Shinn MD, Kirchoff TA, Smith LK, Wilder RE (1986) Measurements of losses and lasing efficiency in GSGG-Cr, Nd and YAG-Nd laser rods. Appl Opt 25:4294–4305
17. Harrison J, Welford D, Moulton PF (1989) Threshold analysis of pulsed lasers with application to a room-temperature Co-MgF_2 laser. IEEE J Quantum Electron 25:1708–1711
18. Welford D, Moulton PF (1988) Room-temperature operation of a Co-MgF_2 laser. Opt Lett 13:975–977
19. Walling JC, Jenssen HP, Morris RC, Odell EW, Peterson OG (1979) Broad-band tuning of solid-state Alexandrite laser. J Opt Soc Am 69:373
20. Walling JC, Peterson OG (1980) High-gain laser performance in Alexandrite. IEEE J Quantum Electron 16:119–120
21. Walling JC, Peterson OG, Jenssen HP, Morris RC, Odell EW (1980) Tunable alexandrite lasers. IEEE J Quantum Electron 16:1302–1315
22. Moulton PF (1986) Spectroscopic and laser characteristics of Ti-Al_2O_3. J Opt Soc Am B Opt Phys 3:125–133

23. Tsuiki H, Kitazawa K, Masumoto T, Shiroki K, Fueki K (1980) Single-crystal growth of pure and Nd-doped Y_2O_3 by floating zone method with Xe arc lamp imaging furnace. J Cryst Growth 49:71–76
24. Tsuiki H, Masumoto T, Kitazawa K, Fueki K (1982) Effect of point-defects on laser oscillation properties of Nd-doped Y_2O_3. Jpn J Appl Phys Part 1 Regul Papers Short Notes Rev Papers 21:1017–1021
25. Ebendorffheidepriem H, Seeber W, Ehrt D (1993) Dehydration of phosphate-glasses. J Non-Cryst Solids 163:74–80
26. Heumann E, Ledig M, Ehrt D, Seeber W, Duczynski EW, Vanderheide HJ et al (1988) CW laser action of Er^{3+} in double sensitized fluoroaluminate glass at room-temperature. Appl Phys Lett 52:255–256
27. Ledig M, Heumann E, Ehrt D, Seeber W (1990) Spectroscopic and laser properties of Cr^{3+}, Yb^{3+}, Er^{3+} fluoride phosphate-glass. Opt Quant Electron 22:S107–S122
28. Seeber W, Ehrt D, Ebendorffheidepriem H (1994) Spectroscopic and laser properties of Ce^{3+}-Cr^{3+}-Nd^{3+} co-doped fluoride phosphate and phosphate-glasses. J Non-Cryst Solids 171:94–104
29. Geusic JE, Marcos HM, Vanuitert LG (1964) Laser oscillation in Nd-doped yttrium aluminium, yttrium gallium and gadolinium garnets. Appl Phys Lett 4:182–184
30. Deshazer LG, Komai LG (1965) Fluorescence conversion efficiency of neodymium glass. J Opt Soc Am 55:940
31. Kushida T, Geusic JE, Marcos HM (1968) Optical properties of YAIG-Nd^{3+}. IEEE J Quantum Electron 4:316
32. Kushida T, Marcos HM, Geusic JE (1968) Laser transition cress section and fluorescence branching ratio for Nd^{3+} in yttrium aluminum garnet. Phys Rev 167:289
33. Pan YB, Li J, Jiang XB (2013) Advanced optical functional transparent ceramics. Science Press, Beijing
34. Silvfast WT (2004) Laser fundamentals. Cambridge University Press, Cambridge
35. Greskovich C, Chernoch JP (1974) Improved polycrysalline ceramic lasers. J Appl Phys 45:4495–4502
36. Greskovich C, Woods KN (1973) Fabrication of transparent ThO_2-doped Y_2O_3. Am Ceram Soc Bull 52:473–478
37. Greskovich C, Woods KN (1972) Recent advances in processing of thorium-doped yttrium oxide ceramics. Am Ceram Soc Bull 51:326
38. Miles GD, Sambell RAJ, Rutherfo J, Stephens GW (1967) Fabrication of fully dense transparent polycrystalline magnesia. Trans Br Ceramic Soc 66:319
39. Rice RW (1971) Hot-pressing of MgO. J Am Ceram Soc 54:205–207
40. Greskovich C, Curran MJ, Oclair CR (1972) Preparation of transparent Y_2O_3-doped ThO_2. J Am Ceram Soc 55:324–325
41. Greskovich C, Brewer JA (2001) Solubility of magnesia in polycrystalline alumina at high temperatures. J Am Ceram Soc 84:420–425
42. Scott C, Kaliszewski M, Greskovich C, Levinson L (2002) Conversion of polycrystalline Al_2O_3 into single-crystal sapphire by abnormal grain growth. J Am Ceram Soc 85:1275–1280
43. Liu WB, Li J, Jiang BX, Zhang D, Pan YB (2012) 2.44 KW laser output of Nd:YAG ceramic slab fabricated by a solid-state reactive sintering. J Alloy Compd 538:258–261
44. Rahaman MN (2003) Ceramic processing and sintering, 2nd edn. CRC Press, New York
45. Ikesue A, Furusato I, Kamata K (1995) Fabrication of polycrystalline transparent YAG cramics by solid-state reaction method. J Am Ceram Soc 78:225–228
46. Li HL, Liu XJ, Huang LP (2005) Fabrication of transparent cerium-doped lutetium aluminum garnet (LuAG:Ce) ceramics by a solid-state reaction method. J Am Ceram Soc 88:3226–3228
47. Li HL, Liu XJ, Huang LP (2006) Fabrication of transparent Ce:LuAG ceramics by a solid-state reaction method. J Inorg Mater 21:1161–1166
48. Li J, Chen Q, Yang LL, Feng GY, Wu WJ, Zheng FS et al (2011) High transmittance of Nd-doped YAG transparent ceramics prepared by solid-state reaction method. Ferroelectrics 411:62–68

49. Wang NL, Zhang XY, Jiang HT, Dong TT, Yang D (2012) Fabrication of Er^{3+}/Yb^{3+} co-doped Y_2O_3 transparent ceramics by solid-state reaction method and its up-conversion luminescence. Mater Chem Phys 135:709–713
50. Wu YS, Li J, Qiu FG, Pan YB, Liu Q, Guo JK (2006) Fabrication of transparent Yb, Cr:YAG ceramics by a solid-state reaction method. Ceram Int 32:785–788
51. Lu J, Prabhu M, Song J, Li C, Xu J, Ueda K et al (2000) Optical properties and highly efficient laser oscillation of Nd:YAG ceramics. Appl Phy B Lasers Opt 71:469–473
52. Arabgari S, Malekfar R, Motamedi K (2011) Parameters effects on the surface morphology and structure of Nd:YAG nanopowders synthesized by co-precipitation method. J Nanopart Res 13:597–611
53. Chen JY, Shi Y, Shi JL (2004) Synthesis of (Y, Gd)2O3: Eu nanopowder by a novel co-precipitation processing. J Mater Res 19:3586–3591
54. Huang YH, Jiang DL, Zhang JX, Lin QL (2009) Precipitation synthesis and sintering of lanthanum doped yttria transparent ceramics. Opt Mater 31:1448–1453
55. Huang ZG, Sun XD, Xiu ZM, Chen SW, Tsai CT (2004) Precipitation synthesis and sintering of yttria nanopowders. Mater Lett 58:2137–2142
56. Ji XB, Deng JG, Kang B, Huang H, Wang X, Jing W et al (2013) Thermal decomposition of $Y_3Al_5O_{12}$ precursor synthesized by urea homogeneous co-precipitation. J Anal Appl Pyrol 104:361–365
57. Li HL, Liu XJ, Xie RJ, Zeng Y, Huang LP (2006) Fabrication of transparent cerium-doped lutetium aluminum garnet ceramics by co-precipitation routes. J Am Ceram Soc 89:2356–2358
58. Ikegami T, Li JG, Mori T, Moriyoshi Y (2002) Fabrication of transparent yttria ceramics by the low-temperature synthesis of yttrium hydroxide. J Am Ceram Soc 85:1725–1729
59. Li JG, Ikegami T, Mori T (2003) Fabrication of transparent Sc_2O_3 ceramics with powders thermally pyrolyzed from sulfate. J Mater Res 18:1816–1822
60. Guo K, Chen HH, Guo XG, Yang XX, Xu FF, Zhao JT (2010) Morphology investigation of yttrium aluminum garnet nano-powders prepared by a sol–gel combustion method. J Alloy Compd 500:34–38
61. Li DY, Hui Y, Lian JS, Xie TT (2005) Progress in research on nanometer Al_2O_3 fabricated by sol–gel method. J Rare Earths 23:600–605
62. Biswas A, Prabhakaran K, Gokhale NM, Sharma SC (2007) Synthesis of nanocrystalline yttria doped ceria powder by urea-formaldehyde polymer gel auto-combustion process. Mater Res Bull 42:609–617
63. Prabhakaran K, Patil DS, Dayal R, Gokhale NM, Sharma SC (2009) Synthesis of nanocrystalline magnesium aluminate ($MgAl_2O_4$) spinel powder by the urea-formaldehyde polymer gel combustion route. Mater Res Bull 44:613–618
64. Su J, Miao J-h, Xu L-h, Ji Y-q, Wang C-q (2012) Synthesis and characterization of nanocrystalline Nd^{3+}-doped gadolinium scandium aluminum garnet powders by a gel-combustion method. Mater Res Bull 47:1709–1712
65. Wang N, Zhang X, Bai Z, Sun H, Liu Q, Lu L et al (2011) Synthesis of nanocrystalline ytterbium-doped yttria by citrate-gel combustion method and fabrication of ceramic materials. Ceram Int 37:3133–3138
66. Huang BT, Ma YQ, Qian SB, Zou D, Zheng GH, Dai ZX (2014) Luminescent properties of low-temperature-hydrothermally-synthesized and post-treated YAG: Ce (5 %) phosphors. Opt Mater 36:1561–1565
67. Moore CA, McMillen CD, Kolis JW (2013) Hydrothermal growth of single crystals of $Lu_3Al_5O_{12}$ (LuAG) and its doped analogues. Cryst Growth Des 13:2298–2306
68. Qian S, Ma Y, Zan F, Zou D, Dai Z, Zheng G et al (2013) Fine YAG:Ce^{3+} nanoparticles synthesised by supercritical hydrothermal reaction. Micro Nano Lett 8:201–205
69. Mancic L, Lojpur V, Marinkovic BA, Dramicanin MD, Milosevic O (2013) Hydrothermal synthesis of nanostructured Y_2O_3 and $(Y_{0.75}Gd_{0.25})_2O_3$ based phosphors. Opt Mater 35:1817–1823

70. Sang YH, Qin HM, Liu H, Zhao LL, Wang YN, Jiang HD et al (2013) Partial wet route for YAG powders synthesis leading to transparent ceramic: a core-shell solid-state reaction process. J Eur Ceram Soc 33:2617–2623
71. Ballato J, Serivalsatit K (2011) Sub-micron grained highly transparent sesquioxide ceramics: synthesis, processing, and properties. In: Laser Technology for Defense and Security Vii. 8039
72. Kokuoz BY, Serivalsatit K, Kokuoz B, Geiculescu O, McCormick E, Ballato J (2009) Er-doped Y_2O_3 nanoparticles: a comparison of different synthesis methods. J Am Ceram Soc 92:2247–2253
73. Serivalsatit K, Ballato J (2010) Submicrometer grain-sized transparent erbium-doped scandia ceramics. J Am Ceram Soc 93:3657–3662
74. Serivalsatit K, Kokuoz B, Yazgan-Kokuoz B, Kennedy M, Ballato J (2010) Synthesis, processing, and properties of submicrometer-grained highly transparent yttria ceramics. J Am Ceram Soc 93:1320–1325
75. Serivalsatit K, Kokuoz BY, Kokuoz B, Ballato J (2009) Nanograined highly transparent yttria ceramics. Opt Lett 34:1033–1035
76. Fedyk R, Hreniak D, Lojkowski W, Strek W, Matysiak H, Grzanka E et al (2007) Method of preparation and structural properties of transparent YAG nanoceramics. Opt Mater 29:1252–1257
77. Pazik R, Gluchowski P, Hreniak D, Strek W, Ros M, Fedyk R et al (2008) Fabrication and luminescence studies of Ce:$Y_3Al_5O_{12}$ transparent nanoceramic. Opt Mater 30:714–718
78. Koechner W (2006) Solid-state laser engineering, 6th edn. Springer, Berlin
79. Shannon RD (1976) Revised effective ionic radii and systematic studies of interatomic distances in halides and chalcogenides. Acta Crystallogr Sect A 32:751–767
80. Siegman AE (1986) Lasers. University Science Books, Sausalito
81. Powell RC (1988) Physics of solid state laser materials. Springer, New York
82. Henderson B, Bartram RH (2000) Crystal field engineering of solid-state laser materials. Cambridge University Press, Cambridge
83. Svelto O (2010) Principles of lasers, 5th edn. Springer, New York
84. Carter CB, Norton MG (2007) Ceramics materials: science and engineering. Springer, Berlin
85. Aldinger F, Claussen N, Kaneno M, Koumoto K, Sōmiya S, Spriggs RM et al (2003) Handbook of advanced ceramics: volume II processing and their applications. Elsevier, Amsterdam
86. Barsoum MW (2003) Fundamentals of ceramics. Institute of Physics Publishing (IoP), UK
87. Pan YB, Li J, Jiang BX (2013) Advanced optical functional transparent ceramics. Science Press, Beijing